Proceedings of the ASME 2024
International Mechanical Engineering Congress and Exposition
IMECE2024
November 17-November 21, 2024, Portland, OR

IMECE2024-143153

STRUCTURAL HEALTH MONITORING OF WIND TURBINE BLADES UTILIZING GUIDED WAVES

Runye Lu
University of Michigan-Shanghai Jiao Tong University Joint Institute, Shanghai Jiao Tong University, Shanghai, China

Yanfeng Shen
University of Michigan-Shanghai Jiao Tong University Joint Institute, Shanghai Jiao Tong University, Shanghai, China

ABSTRACT

Wind turbine blades (WTBs), as crucial components of wind turbine generators, are susceptible to structural damage due to severe weather conditions during operation periods. This paper proposes an active structural health monitoring (SHM) system, leveraging guided waves for the WTBs diagnosis. It comprises electro-magnetic actuators, piezoelectric sensing units, and data acquisition and signal processing modules. An algorithm incorporating spectral wave energy and cross-correlation is developed for precise damage detection. To validate the system and algorithm, a simplified SHM system is implemented on a laboratory-scale WTB prototype. Artificial damage simulated by the bonded mass block can be accurately detected and located. For the subsequent phase, a full-scale test is conducted on a XX-192 WTB (anonymity of XX for confidential purpose), exceeding 90 meters in length and fixed on a foundation tower as a cantilever beam under fatigue tests. The practical durability and stability of the system is demonstrated, subjected to over 500,000 flapping and edging cyclic loadings. The system precisely detects the artificial delamination in the fashion of a bonded composite sample on the WTB, achieving the detection of a small delamination area of 80 mm 30 mm. The paper culminates in summary, concluding remarks, and suggestions for future work.*

Keywords: structural health monitoring; guided waves; wind turbine blades; piezoelectric active wafer sensors; active sensing

1. INTRODUCTION

Wind power, as a renewable clean energy, has enacted an imperative role in the global effort of mitigating carbon emission, reducing reliance on fossil fuel resources, and diversifying energy portfolios [1, 2]. In recognition of its paramount significance, enormous wind turbine generators (WTGs) have been deployed on a large scale across diverse terrains and geographical regions, spanning ocean, dessert, and mountainous landscapes. The extreme weather conditions, such as gales, freezing conditions, lightning strikes, and sandstorms, pose formidable safety hazards to WTGs components [3]. Wind turbine blades (WTBs), as crucial components for transferring the wind power into electrical energy, comprise 15%-20% percent of the manufacture and maintenance expense [4-6]. The incipient damage of blades is detrimental to power generating efficiency, and is prone to severe damage, triggering catastrophic hazards for adjacent components or even the whole WTG [3, 7]. Typical damage types occurring on WTBs mainly include cracks, adhesively/skin debonding, buckling, delamination, edge erosion and so on [8, 9]. The subsequent consequences, like power generation loss, high maintenance expenditures, life security issues, necessitate Nondestructive Evaluation (NDE) and Structural Health Monitoring (SHM) strategies for early-stage damage detection [8, 10-12].

A wide spectrum of damage detection technologies has been developed for the inspection of WTBs [13-15], encompassing strain measurement [16, 17], acoustic emission [18, 19], ultrasonic/vibration-based methodologies [20-25], optical fiber sensor techniques [26], thermography [27, 28], machine vision [16], etc. To exemplify, inspection methods based on strain gauges are utilized to continuously track subtle alterations in length or deformations of the WTBs under the applied loads. In comparison to conventional strain gauges, optical fiber sensors are immune to electrical and magnetic interferences, converting geometric and material changes into optical properties variations [29]. Moreover, the thermography diagnosis aims at the detection of thermodynamic properties of the turbine blades, enabling a large scanning coverage of WTBs surface. Regarding the machine vision based technique, it employs sequences of 2-dimensional/3-dimensional images from various locations and perspectives to evaluate health status of target structures [1].

Among state-of-the-art methodologies, emphasis is directed towards the most relevant ultrasonics and vibrations based methods. Acoustic emission (AE) techniques utilize transient elastic waves triggered by the release of energy from damage

initiation, crack propagation, and plastic deformation [19]. SHM systems based on AE technique are deployed in critical areas of WTB surfaces, capturing micro-scale material changes in WTB resulting from the occurrence, propagation, and failure of the blade [30]. However, enormous AE sensors are demanded to be installed neighboring the location of the potential blade damage, presenting considerable logistic challenges [7]. Moreover, the data acquisition hardware with high sampling frequency is essential for the accurate diagnosis, usually entailing bulky and expensive equipment. Challenges also arise from the difficulty in distinguishing informative AE signals from the environmental noise [31].

Damage detection methods based on ultrasonics exploit distinctive features like reflection, attenuation, resonance, and transmission patterns for anomaly detection, facilitating the evaluation of damage existence, location, and severity. The ultrasonic methodologies are pervasively employed for investigating intermediate structural damage, like delamination, debonding, ice accumulation [32], etc. [5, 31]. Furthermore, nonlinear ultrasonics techniques exhibit the capacity to augment accuracy and detect incipient damage at nascent stages [33]. Nevertheless, the limitations of ultrasonic based methods lie in the requirement for complicated hardware configurations, a larger abundance of sensors, and complex signal processing [7].

Regarding the vibration-based methods, the structural dynamic properties, such as frequency spectra, modal parameters, natural frequencies, mode shapes, and damping characteristics, serve as key indicators for anomaly detection [34-36]. Various accelerometers are embraced for their ability to capture a wide frequency band. Signal processing techniques including wavelet transform [37], short time Fourier transform (STFT), empirical mode decomposition (EMD) [8, 36], support vector machines (SVM) [38], hidden Markov models (HMM) [39], and other classifier-based methods and features extraction techniques are considered as potent tools for the WTB damage detection [7]. However, the extraction and identification of the effective damage signals amidst varying environmental and operating conditions remain an uncharted issue. Furthermore, vibration-based methods primarily target large-scale damage types instead of incipient damage, and function passively without the capability of tracing the progressing of damage.

Addressing the limitations and disadvantages inherent in the aforementioned methods, this paper proposes an active SHM system for WTBs leveraging guided waves and vibrations. This system harnesses cost-effective flexible piezoelectric sensing units (20-70 pieces at a mere 3 dollar per piece), forming a dense sensing array. This array enables extensive inspection coverage, spanning over 60 meters and typically encompassing more than half of the WTB's length. Besides, a self-calibrated electro-magnetic actuator is developed to generate the impulse excitation to the WTB structure at will, propagating exceeding 15 meters, and being captured by the distributed sensing units. This method utilizes the middle frequency band to mitigate low frequency environmental disturbances and the limited propagation capability of high frequency waves. Simultaneously, such frequency band can ensure the damage detection accuracy, enabling the diagnosis of incipient damage types occurring at initial stages. Therefore, the developed system can endow WTBs with the active sensing and diagnosis capability, guarding against the catastrophic damage scenarios, thus reducing the maintenance expenditures.

This paper commences with the introduction of the active SHM system for WTBs, outlining the components including the actuator, sensor, and other hardware equipment. Subsequently, the feasibility of the active system is validated on a 3.4 meters WTB, considered as the experimental prototype. The comprehensive algorithm proves to be effective on the prototype WTB for the detection and localization of the artificial damage. For the next phase, a full-scale test is implemented on a WTB over 90 meters in length under fatigue tests. The spectral energy distribution is utilized to visualize and trace the overall health conditions of the WTB. Ultimately, the artificial debonding are fabricated and evaluated, culminating in a thorough assessment of the system's capabilities.

2. ACTIVE SHM SYSTEM FOR WTBS

This section establishes an active SHM framework for the WTBs. The hardware of the system comprises self-calibrated actuator, flexible piezoelectric sensing array, data acquisition equipment, computation device, and control system, as illustrated in Figure 1. The integrated box can actively control the actuators to deliver impulse waves to WTBs, which will then be captured by the distributed sensing array. The informative signals are processed and exploited for the damage diagnosis.

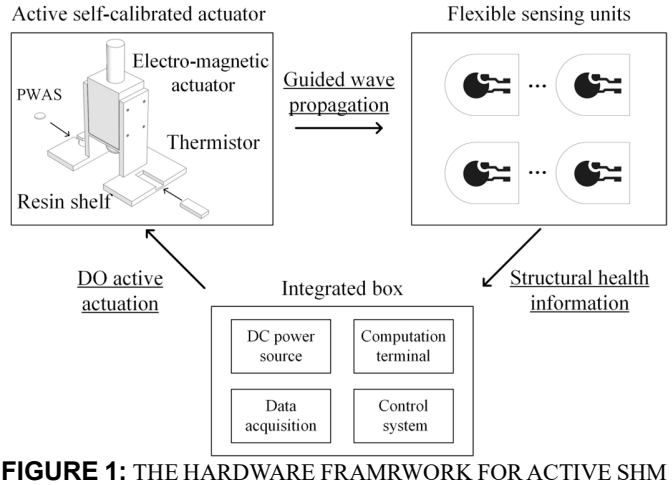

FIGURE 1: THE HARDWARE FRAMRWORK FOR ACTIVE SHM SYSTEM

The actuators can be affixed onto the WTB surfaces to excite guided waves, propagating across the target structure, and gradually attenuating after traversing 15 meters. The sensor units will be bonded on the WTB materials and capture the actuation signals, as shown in Figure 2. A typical set of temporal and frequency spectral signals captured from the sensor located 8 meters away from the actuator is displayed in Figure 3. The sensing signal resembles a typical impulse with a duration of

0.03 s, and the frequency component mainly range from 0-5000 Hz in the specific scenario.

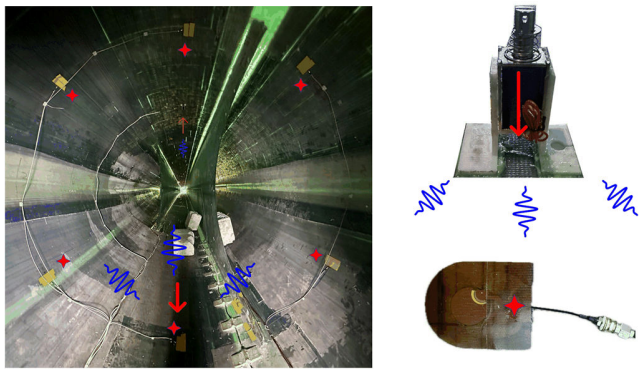

FIGURE 2: THE PRACTICAL ACTUATOR AND SENSOR DEPLOYMENT IN WTB INNER SURFACE

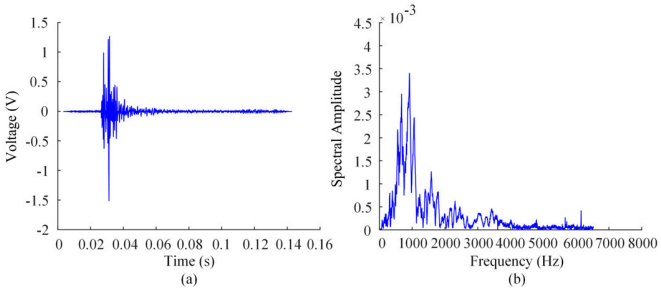

FIGURE 3: THE TYPICAL (A) TEMPORAL AND (B) FREQUENCY DOMAIN SIGNAL CAPTURED BY THE SENSOR

Apart from actuators and sensors, the practical configurations of the integrated box are displayed in Figure 4. The DC power can output a 12V electrical supply to the active actuators. The data acquisition system possesses 64 channels with a total sampling frequency of 500 kHz, and is connected to the industrial PC terminal by the PCIe port. All these components constitute an efficient, cost-effective, portable hardware system for the health monitoring of WTBs.

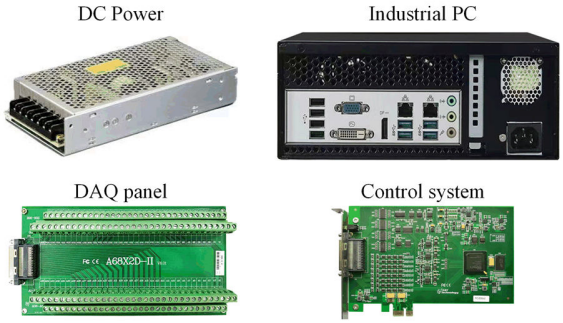

FIGURE 4: PRACTICAL SYSTEM SETTINGS OF THE INTEGRATED BOX

3. EXPERIMENTAL IMPLEMENTATION ON A WTB PROTOTYPE

This section implements the active SHM system on a WTB prototype with 3.4 meters in length, from the FD7.0-10 KW wind turbine generator. The comprehensive algorithm based on linear guided wave features is developed for the damage detection and localization.

3.1 Experimental Configurations

Regarding the experimental settings, the WTB was fixed on the shelf with six bolts. 11 miniaturized sensing elements were bonded on the outer surface of the WTB while an active actuator was affixed at the center of the blade to deliver the impulse waves. The actuation was repeated for 20 times to avoid stochastic disturbance. The sensing units were connected to the DAQ panel by co-axial cables.

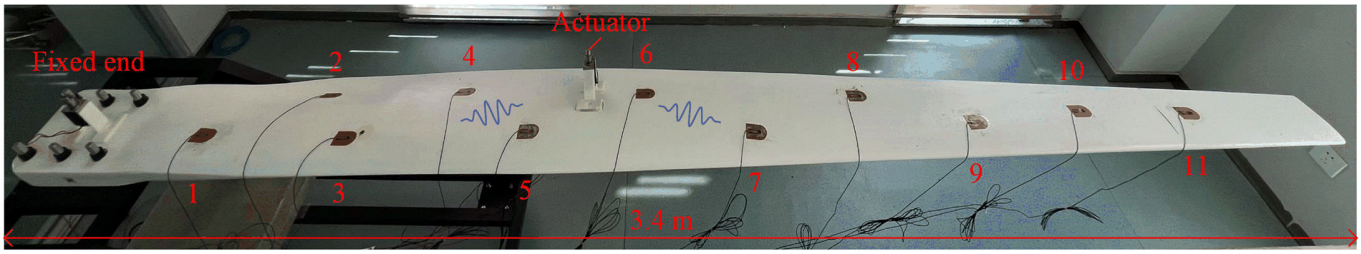

FIGURE 5: SENSOR AND ACTUATOR CONFIGURATIONS FOR THE WTB PROTOTYPE

Since the typical damage types like delamination, crack, and debonding are destructive and inversible, the experimental damage was simulated by the damping clay bonded at different locations on the WTB surface. The simulated damage, functioning akin to mass blocks, modified the local material and geometric properties, thereby inducing attenuation of waves and vibrations. In this test, 10 mass blocks were artificially distributed surrounding each sensing unit for damage localization. It is worth mentioning that sensor #11 was not employed due to cause of force majeure.

3.2 Damage Diagnosis

After initial analyses on the raw wave signals, it was discerned that signals with frequencies exceeding 2500 Hz exhibited heightened sensitivity to the presence of mass blocks. Therefore, a high pass frequency filter was utilized to extract the most informative components. Regarding the specific cases for

the damage deployed near sensor #3 and sensor #7, the temporal signals and frequency spectra of two typical sensors closed to the damage and away from the damage are presented in Figure 6 and Figure 7.

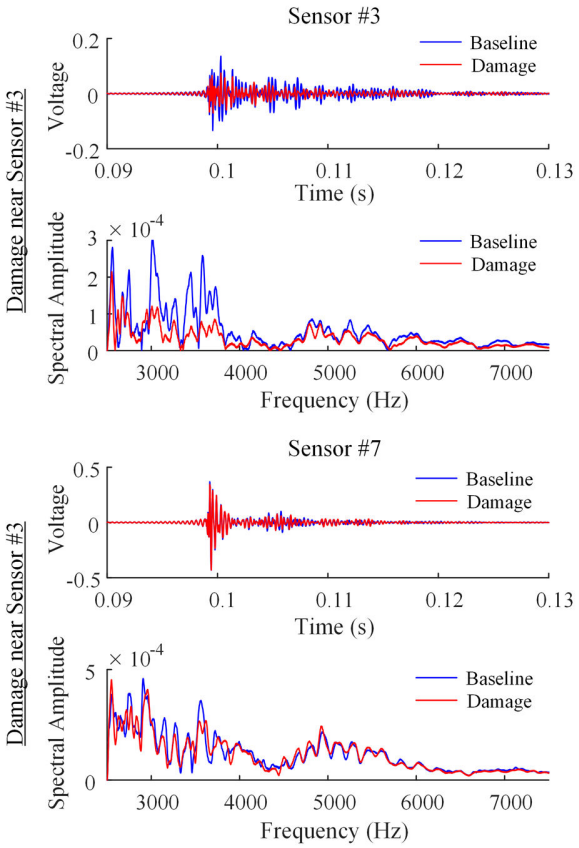

FIGURE 6: TEMPORAL SIGNALS AND FREQUENCY SPECTRA FOR SENSOR #3 AND SENSOR #7 WITH THE DAMAGE DEPLOYED NEAR SENSOR #3

Notably, in Figure 6, for the sensing units #3 closed to the damage site, the propagating wave signals encounter obvious attenuation with the existence of the mass block. Regarding the sensor #7 away from the damage, there is only slight and subtle alteration of the damage signal compared with the baseline signal. Situations are similar for the signals in Figure 7.

For further detection and localization of the damage, several damage correlated indices based on linear guided wave theory were utilized, encompassing spectral energy change rate, spectral correlation coefficient (*CC)*, etc., the formulas of which are listed below:

$$\Delta E = \left(E_2 - E_1\right)/E_1 = \left(\int_{f_1}^{f_2} \hat{x}_2(f)df - \int_{f_1}^{f_2} \hat{x}_1(f)df\right) \Big/ \int_{f_1}^{f_2} \hat{x}_1(f)df \quad (1)$$

$$CC = 1 - \frac{\left|\int_{f_1}^{f_2} \hat{x}_1(f)\hat{x}_2(f)df\right|}{\sqrt{\int_{f_1}^{f_2} \hat{x}_1^2(f)df \int_{f_1}^{f_2} \hat{x}_2^2(f)df}} \quad (2)$$

where E represents the spectral energy; $\hat{x}(f)$ denotes the Fourier transform results; the subscript 1 signifies the pristine case while subscript 2 represents the damaged case.

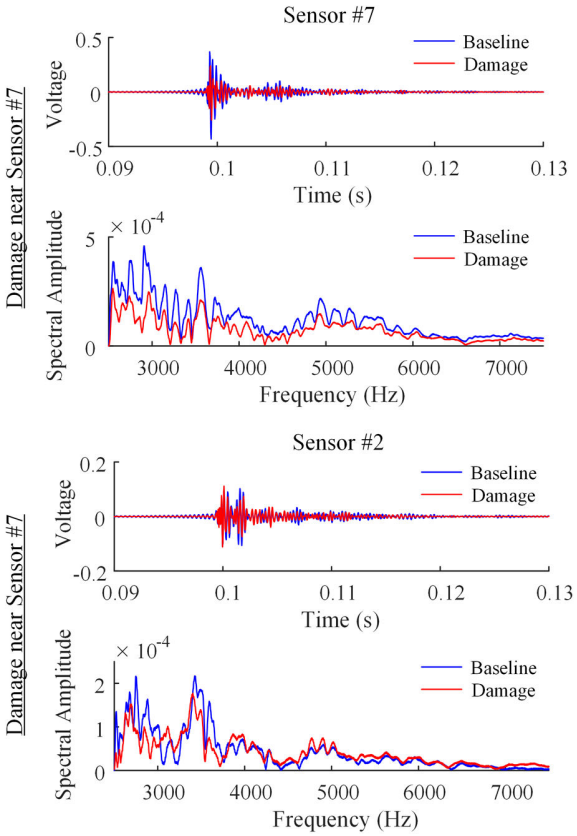

FIGURE 7: TEMPORAL SIGNALS AND FREQUENCY SPECTRA FOR SENSOR #7 AND SENSOR #2 WITH DAMAGE DEPLOYED NEAR SENSOR #7

Subsequently, the damage indices are displayed for all the sensors with the damage deployed near sensor #3 and sensor#7 respectively, corresponding to the previous cases, as shown in Figure 8 and Figure 9. Regarding the spectral energy, an obvious decrease can be observed for the sensors neighboring the damage site. The relative change rate of the spectral energy denotes the attenuation resulting from the mass block. Among all the sensing units, the sensor closest to the damage reveals largest attenuation for both damage cases, as highlighted in the second subplot. The spectral correlation coefficient quantifies the signal deviation between the baseline and damage. The *CC* indices for the sensors located leftwards or rightwards are influenced by the existence of the damage. Specifically, *CC* indices manifest an increment for sensor #1-#4 due to damage neighboring sensor #3. *CC* indices for sensor #8- #10 display an increment with damage appearing near sensor #7. Therefore, both indices can coordinate with each other to further detect and localize the damage existence. A threshold value for both indices can be determined for the practical application.

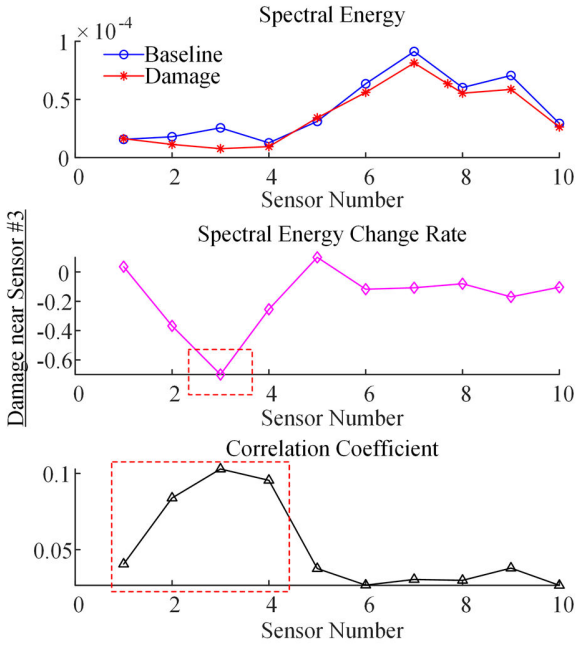

FIGURE 8: THE SPECTRAL ENERGY, ITS CHANGING RATE, AND CORRELATION COEFFICIENT FOR DAMAGE NEAR SENSOR #3

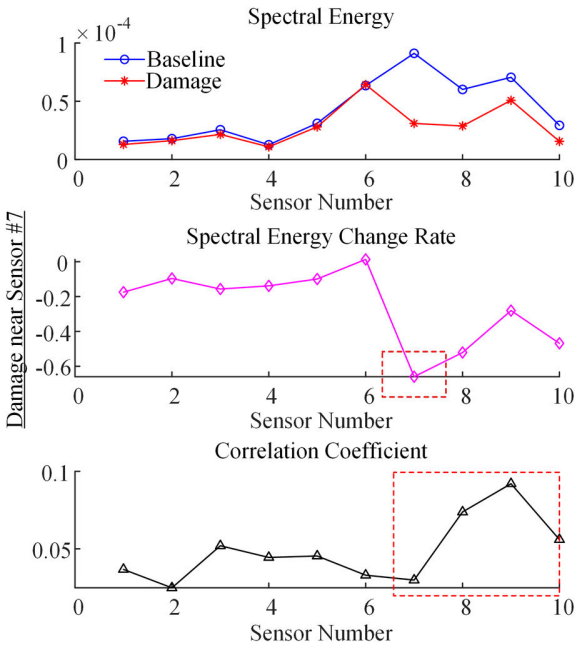

FIGURE 9: THE SPECTRAL ENERGY, ITS CHANGING RATE, AND CORRELATION COEFFICIENT FOR DAMAGE NEAR SENSOR #7

4. PRACTICAL DEMONSTRATION OF ACTIVE SHM SYSTEM FOR THE XX-192 WTB

This section elucidates the practical implementation of the active SHM system on the XX-192 WTB, spanning over 90 meters in length, during prolonged fatigue tests. Through these rigorous assessments, the system's feasibility and durability are validated. The system demonstrates its capability to trace the fatigue test and evaluate the artificially induced delamination, promptly identifying anomalies that arise during the fatigue tests.

4.1 Configurations of Fatigue Tests on WTB

The practical demonstration of the SHM system is implemented on a WTB over 90 meters at a test tower subjected to cyclic fatigue loadings. The configuration of the fatigue test is displayed in Figure 10. The WTB is suspended to a fixed tower, resembling a cantilever beam. The yellow clamp fixtures with inertial devices are utilized to initiate the cyclic loadings. The endurance and reliability of the actuator and sensor system were meticulously evaluated over the course of 1 million fatigue loadings spanning a duration of 3 months. This rigorous testing regimen ensured the robustness and longevity of the SHM system under practical operational conditions.

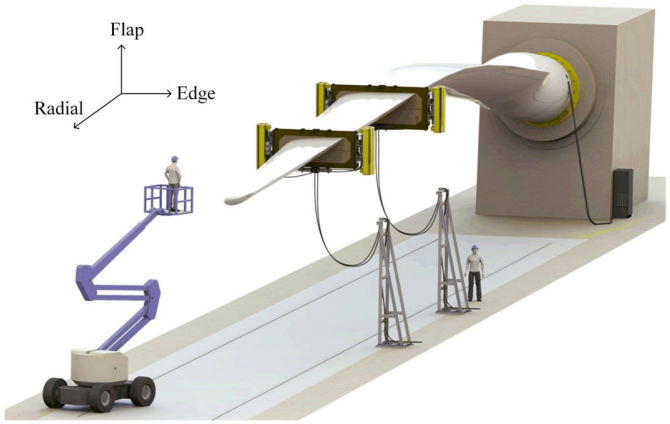

FIGURE 10: THE PRACTICAL CONFIGURATIONS OF THE FATIGUE TEST (IN COURTESY OF MTS SYSTEM)

The actuators and sensors configurations are illustrated in Figure 11. For this XX-192 WTB, altogether 64 sensing units and 4 actuators were strategically deployed in 11 cross sections, spanning the initial 50 meters of the WTB with a 5-meter interval. Within each cross section (except the last one), 6 sensors were bonded at diverse typical regions such as GFRP, girder, web, leading edge, and tailing edge, shown in Figure 2 and Figure 11. The deployment of the 4 actuators was orchestrated: two were positioned at 10 m and 30 m within the middle chamber, while the other two were situated at 20 m and 40 m along the leading edge. This configuration ensures optimal wave propagation throughout the targeted length of the WTB. In practical implementation, the 4 actuators are sequentially activated, with each imparting impulse to the WTB for 20 times consecutively.

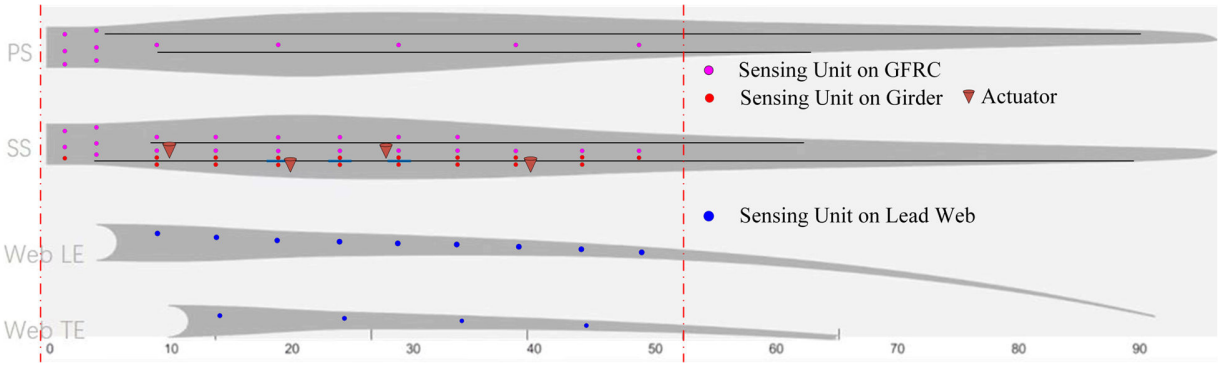

FIGURE 11: THE DEPLOYMENT DIAGRAM OF ACTUACTORS AND SENSORS INSIDE THE BLADE

4.2 Wave Propagation and Damage Detection

To visualize the wave propagation in the WTB, the spectral energy of sensors is displayed in Figure 12. Altogether 54 sensors spanning from 5 m to 45 m along the WTB are selected and divided into 4 regions by the 4 actuators. It should be mentioned that the first 6 sensors are utilized for artificial damage monitoring in next section, and the last 4 sensing units are omitted due to formatting constraints. It can be observed from Figure 12 that the impulse wave generated by each actuator can traverse across 15 m to 20 m in the blade. Consequently, multiple sensors within specific regions assigned to a single actuator are tasked with monitoring distinct areas, as outlined in Table 1. Another intriguing phenomenon is that the third sensor at each section possesses largest spectral energy, bonded on the GFRP surface in the middle chamber as shown in Figure 2. Such phenomenon can be validated by wave propagation signals for the six sensors at one typical cross section, illustrated in Figure 13. This indicates that the GFRP components of the WTB are suitable for impulse wave transmission, serving as the guidance for sensor configurations for subsequent test.

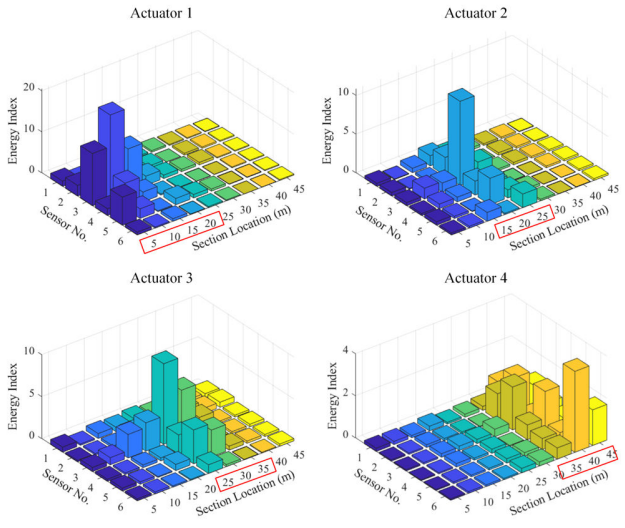

FIGURE 12: THE ENERGY DISTRIBUTION OF 54 SENSORS COVERING 5-45 METERS OF THE WTB FOR 4 ACTUATORS

TABLE 1: SENSOR NUMBER CORRESPONDING TO THE ACTUATOR AND SECTION LENGTH

Actuator	Sensor	Section
No.1: 10m	#7-#24	5 m-20 m
No.2: 20m	#19-#36	15 m-25 m
No.3: 20m	#31-#48	25 m-35 m
No.4: 30m	#43-#60	35 m-45 m

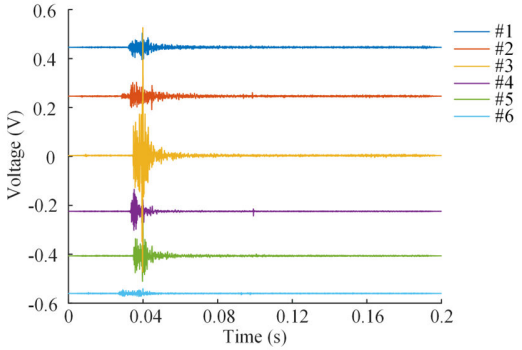

FIGURE 13: WAVE PROPAGATION SIGNALS FOR SIX SENSORS WITHIN ONE CROSS SECTION

In order to trace the spectral energy evolution with the fatigue tests processing, the energy bar plot of the sensor #31-#48 (belonging to actuator #3's monitoring regions) with measurement time is displayed in Figure 14. The measurement was conducted approximately in a three-day interval for 8 times, covering the cyclic loadings up to 500,000 times. Generally, for the majority of sensors, the spectral energy manifests a gradual and slight downward trend, resulting from the dense and continuous cyclic loadings. Such fatigue tests induce degeneration and degradation in the GFRP materials, the adhesive layers, the structural joints, etc., posing attenuation and scattering to the impulse waves captured by the sensing units. Furthermore, the accidental emergencies can also be detected and alerted by the sudden drop of spectral energy. Notably, the spectral energy remains almost zero due to the artificial damage of the sensor #38

during the maintenance. Similarly, the peeling or destroy of sensors induced by other accidents can be promptly detected.

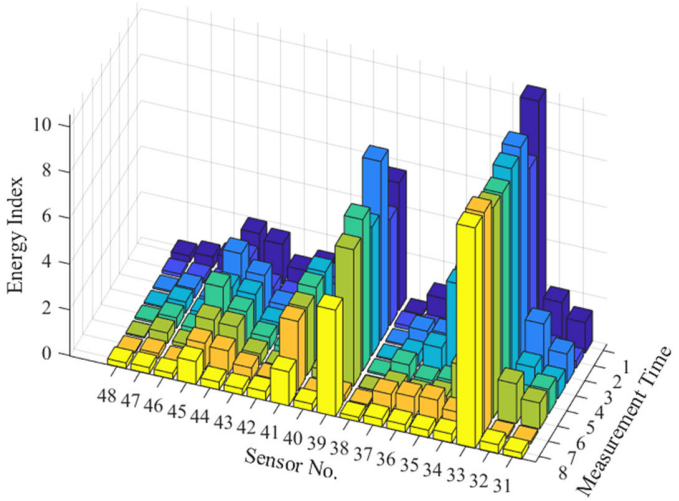

FIGURE 14: THE SPECTRAL ENERGY BAR PLOT OF SENSOR #31-#48 FOR ACTUATOR #3 COVERING 25-30 METERS

To demonstrate the local detection capability, some uni-direction GFEP specimens with prefabricated delamination were bonded on the girder of WTB, as illustrated in Figure 15. During the fatigue test, the prefabricated damage may evolve into larger delamination area. The comparative vibration signals at 8 different measurements (spanning 500,000 cyclic loadings) are displayed in Figure 16 and Figure 17. For the intact specimen, the sensor consistently received effective signals, with the amplitude maintaining a stable value. In comparison, regarding the specimen with delamination, the captured signals remained a normal value until the fifth measurement. The sudden vanishment of signal indicated the existence of delamination in GFRP laminates. The delamination acted as a barrier, trapping waves within the damaged regions, and impeding their transmission to the sensor.

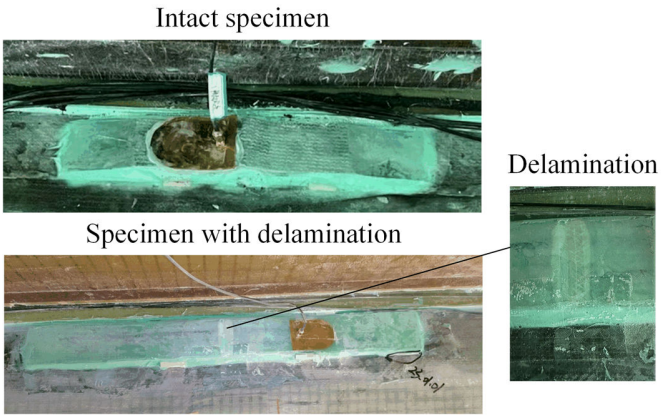

FIGURE 15: THE INTACT AND DAMAGED SPECIMEN BONDED ON THE WTB GIRDER

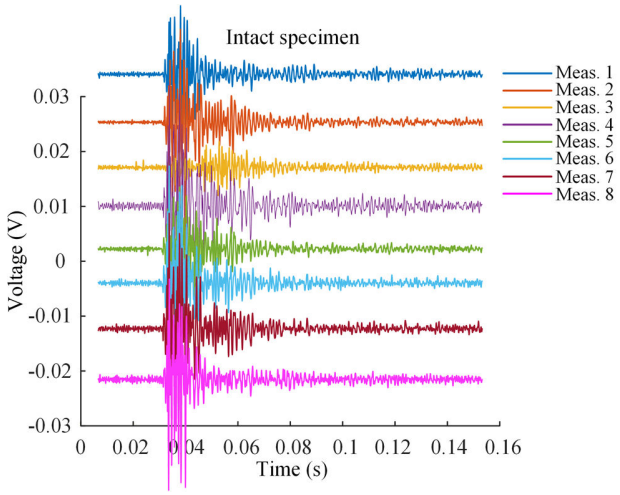

FIGURE 16: VIBRATION SIGNALS AT DIFFERENT MEASUREMENTS FOR THE INTACT SPECIMEN

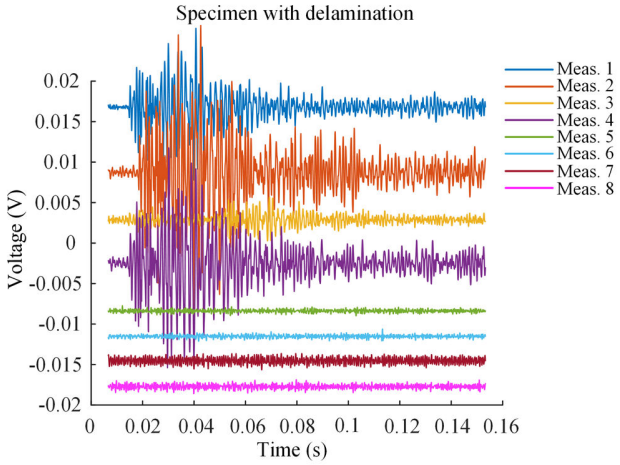

FIGURE 17: VIBRATION SIGNALS AT DIFFERENT MEASUREMENTS FOR SPECIMEN WITH DELAMINATION

5. CONCLUDING REMARKS AND FUTURE WORK

This paper proposed an active SHM system for WTBs exploiting guided waves and vibrations. The active framework comprised actuators, sensors, and integrated DAQ and signal processing modules. The hardware system and the damage diagnosis algorithm were initially validated on the prototype WTB with 3.4 meters in length, demonstrating the capability of damage detection and localization. In the practical implementation of the XX-192 WTB, the durability and stability of the hardware system were verified under 1,000,000 cycles of fatigue loadings. The system succeeded in tracing the fatigue life of WTB through the spectral energy and detected accidental anomalies occurring during the tests. Ultimately, the artificially fabricated delamination in GFRP specimens were accurately investigated.

Currently, the SHM system is under another test on larger WTB over 100 meters. For future work, the system will be deployed on an operating WTB for practical use.

6. ACKNOWLEDGEMENTS

The support from the National Natural Science Foundation of China (contract numbers 51975357) is thankfully acknowledged; this research is also sponsored by the Shanghai Rising-star Program (contract number 21QA1405100).

REFERENCES

[1] Zhou, H. F., Dou, H. Y., Qin, L. Z., Chen, Y., Ni, Y. Q., and Ko, J. M., 2014, "A review of full-scale structural testing of wind turbine blades," Renewable and Sustainable Energy Reviews, 33, pp. 177-187.

[2] Zhou, Y., Wang, S., Ye, R., and Guo, S., 2018, "Assessing national renewable energy competitiveness of the G20: A revised Porter's Diamond Model," Renewable and Sustainable Energy Reviews, 93.

[3] Chou, J.-S., Chiu, C.-K., Huang, I. K., and Chi, K.-N., 2013, "Failure analysis of wind turbine blade under critical wind loads," Engineering Failure Analysis, 27, pp. 99-118.

[4] Liu, W. Y., Tang, B. P., Han, J. G., Lu, X. N., Hu, N. N., and He, Z. Z., 2015, "The structure healthy condition monitoring and fault diagnosis methods in wind turbines: A review," Renewable and Sustainable Energy Reviews, 44, pp. 466-472.

[5] García Márquez, F. P., Tobias, A. M., Pinar Pérez, J. M., and Papaelias, M., 2012, "Condition monitoring of wind turbines: Techniques and methods," Renewable Energy, 46, pp. 169-178.

[6] Yang, R., He, Y., and Zhang, H., 2016, "Progress and trends in nondestructive testing and evaluation for wind turbine composite blade," Renewable and Sustainable Energy Reviews, 60, pp. 1225-1250.

[7] Li, D., Ho, S.-C. M., Song, G., Ren, L., and Li, H., 2015, "A review of damage detection methods for wind turbine blades," Smart Materials and Structures, 24(3).

[8] Du, Y., Zhou, S., Jing, X., Peng, Y., Wu, H., and Kwok, N., 2020, "Damage detection techniques for wind turbine blades: A review," Mechanical Systems and Signal Processing, 141.

[9] Sareen, A., Sapre, C. A., and Selig, M. S., 2014, "Effects of leading edge erosion on wind turbine blade performance," Wind Energy, 17(10), pp. 1531-1542.

[10] Kalkanis, K., Kaminaris, S. D., Psomopoulos, C., and Ioannidis, G. C., 2018, "Structural Health Monitoring for the Advanced Maintenance of Wind Turbin."

[11] Song, G., Li, H., Gajic, B., Zhou, W., Chen, P., and Gu, H., 2013, "Wind turbine blade health monitoring with piezoceramic-based wireless sensor network," International Journal of Smart and Nano Materials, 4(3), pp. 150-166.

[12] Ghoshal, A., Sundaresan, M. J., Schulz, M. J., and Frank Pai, P., 2000, "Structural health monitoring techniques for wind turbine blades," Journal of Wind Engineering and Industrial Aerodynamics, 85(3), pp. 309-324.

[13] Schubel, P. J., Crossley, R. J., Boateng, E. K. G., and Hutchinson, J. R., 2013, "Review of structural health and cure monitoring techniques for large wind turbine blades," Renewable Energy, 51, pp. 113-123.

[14] Yang, B., and Sun, D., 2013, "Testing, inspecting and monitoring technologies for wind turbine blades: A survey," Renewable and Sustainable Energy Reviews, 22, pp. 515-526.

[15] Amenabar, I., Mendikute, A., Lopez-Arraiza, A., Lizaranzu Fernández, M., and Aurrekoetxea, J., 2011, "Comparison and analysis of non-destructive testing techniques suitable for delamination inspection in wind turbine blades," Composites Part B: Engineering, 42, pp. 1298-1305.

[16] Schubel, P., Crossley, R., Boateng, E. K. G., and Hutchinson, J. R., 2013, "Review of structural health and cure monitoring techniques for large wind turbine blades," Renewable Energy, 51, pp. 113-123.

[17] Ozbek, M., and Rixen, D. J., 2013, "Operational modal analysis of a 2.5 MW wind turbine using optical measurement techniques and strain gauges," Wind Energy, 16(3), pp. 367-381.

[18] Bouzid, O. M., Tian, G. Y., Cumanan, K., and Moore, D., 2015, "Structural Health Monitoring of Wind Turbine Blades: Acoustic Source Localization Using Wireless Sensor Networks," Journal of Sensors, 2015, p. 139695.

[19] Liu, P., Xu, D., Li, J., Chen, Z., Wang, S., Leng, J., Zhu, R., Jiao, L., Liu, W., and Li, Z., 2019, "Damage mode identification of composite wind turbine blade under accelerated fatigue loads using acoustic emission and machine learning," Structural Health Monitoring, 19(4), pp. 1092-1103.

[20] Shoja, S., Berbyuk, V., and Boström, A., 2018, Modelling of guided wave propagation for detecting delamination in large composite structures.

[21] Ou, Y., Chatzi, E. N., Dertimanis, V. K., and Spiridonakos, M. D., 2016, "Vibration-based experimental damage detection of a small-scale wind turbine blade," Structural Health Monitoring, 16(1), pp. 79-96.

[22] Tcherniak, D., and Mølgaard, L. L., 2017, "Active vibration-based structural health monitoring system for wind turbine blade: Demonstration on an operating Vestas V27 wind turbine," Structural Health Monitoring: An International Journal, 16(5), pp. 536-550.

[23] Niezrecki, C., Avitabile, P., Chen, J., Sherwood, J., Lundstrom, T., LeBlanc, B., Hughes, S., Desmond, M., Beattie, A., Rumsey, M., Klute, S. M., Pedrazzani, R., Werlink, R., and Newman, J., 2014, "Inspection and monitoring of wind turbine blade-embedded wave defects during fatigue testing," Structural Health Monitoring, 13(6), pp. 629-643.

[24] Ruan, J., Michael Ho, S. C., Patil, D., Li, M., and Song, G., 2014, "Wind turbine blade damage detection using an active sensing approach," Smart Materials and Structures, 23(10).

[25] Choi, S.-W., Farinholt, K. M., Taylor, S. G., Light-Marquez, A., and Park, G., 2014, "Damage Identification of Wind Turbine Blades Using Piezoelectric Transducers," Shock and Vibration, 2014, pp. 1-9.

[26] Alian, H., Konforty, S., Ben-Simon, U., Klein, R., Tur, M., and Bortman, J., 2019, "Bearing fault detection and fault size estimation using fiber-optic sensors," Mechanical Systems and Signal Processing, 120, pp. 392-407.

[27] Yang, B., Zhang, L., Zhang, W., and Ai, Y., "Non-destructive testing of wind turbine blades using an infrared thermography: A review," Proc. 2013 International Conference on Materials for Renewable Energy and Environment, pp. 407-410.

[28] Gómez Muñoz, C. Q., García Márquez, F. P., and Sánchez Tomás, J. M., 2016, "Ice detection using thermal infrared

radiometry on wind turbine blades," Measurement, 93, pp. 157-163.
[29] Li, H.-N., Li, D.-S., and Song, G.-B., 2004, "Recent applications of fiber optic sensors to health monitoring in civil engineering," Engineering Structures, 26(11), pp. 1647-1657.
[30] Tang, J., Soua, S., Mares, C., and Gan, T.-H., 2017, "A Pattern Recognition Approach to Acoustic Emission Data Originating from Fatigue of Wind Turbine Blades," Sensors.
[31] Qiao, W., and Lu, D., 2015, "A Survey on Wind Turbine Condition Monitoring and Fault Diagnosis - Part II: Signals and Signal Processing Methods," IEEE Transactions on Industrial Electronics, 62, pp. 1-1.
[32] Shoja, S., Berbyuk, V., and Boström, A., 2018, "Guided wave–based approach for ice detection on wind turbine blades," Wind Engineering, 42(5), pp. 483-495.
[33] Lu, R., Shen, Y., Zhang, B., and Xu, W., 2023, "Nonlinear Electro-Mechanical Impedance Spectroscopy for fatigue crack monitoring," Mechanical Systems and Signal Processing, 184, p. 109749.
[34] Yan, Y. J., Cheng, L., Wu, Z. Y., and Yam, L. H., 2007, "Development in vibration-based structural damage detection technique," Mechanical Systems and Signal Processing, 21(5), pp. 2198-2211.
[35] Wang, H., and Jing, X., 2017, "Vibration signal–based fault diagnosis in complex structures: A beam-like structure approach," Structural Health Monitoring, 17(3), pp. 472-493.
[36] Abouhnik, A., and Albarbar, A., 2012, "Wind turbine blades condition assessment based on vibration measurements and the level of an empirically decomposed feature," Energy Conversion and Management, 64, pp. 606-613.
[37] Yan, R., Gao, R. X., and Chen, X., 2014, "Wavelets for fault diagnosis of rotary machines: A review with applications," Signal Processing, 96, pp. 1-15.
[38] Laouti, N., Sheibat-Othman, N., and Othman, S., 2011, "Support Vector Machines for Fault Detection in Wind Turbines," IFAC Proceedings Volumes, 44(1), pp. 7067-7072.
[39] Miao, Q., and Makis, V., 2007, "Condition monitoring and classification of rotating machinery using wavelets and hidden Markov models," Mechanical Systems and Signal Processing, 21(2), pp. 840-855.